

Interaction Between Primary and Secondary Waves in a Rotating Detonation Rocket Engine

Guillaume Vignat^a, Davy Brouzet^a, Matthew Bonanni^a, Matthias Ihme^{a,b}

^a Department of Mechanical Engineering, Stanford University

488 Escondido Mall, Stanford, California, United States of America

^b Department of Photon Science, SLAC National Accelerator Laboratory
Menlo Park, CA 94025, USA

1 Introduction

Pressure gain combustion has gained tremendous traction in recent years as a breakthrough technology to improve the efficiency of propulsion and power generation devices [1–3]. The rotating detonation rocket engine (RDRE) has recently been demonstrated as a mechanically simple and cost effective engine design for continuous thrust production in rocket applications. In this engine design, combustion occurs within an annular cavity, into which reactants, commonly a hydrocarbon gaseous fuel and pure oxygen, are continuously injected through the head plane, forming a layer of fresh, partially mixed, combustible mixture through which one or multiple detonation waves propagate in the azimuthal direction, consuming this layer of fresh reactants in a periodic manner. In most applications, the injection system is non-premixed to alleviate the risk of flashback into the upstream manifolds of the reactant delivery system.

The viability of RDREs has been demonstrated in a series of recent experiments, performed at ambient condition on thrust stands and sleds [4–6], under vacuum [7, 8], and recently during space flight [9]. In addition to their mechanical simplicity, RDREs can provide higher volumetric power densities and improved thermodynamic efficiency and thrust compared to traditional, deflagration-based engine designs [2, 3, 10–14]. However, measurements conducted during test firing of RDREs often report thrusts lower than theoretical engine cycle calculations. A number of non-ideal effects manifest during these tests and contribute to a decrease in combustion efficiency and specific impulse. An exhaustive list of these non-ideal effects can be found in a recent review [15]. Of particular interest to the present work are weak secondary waves and unsteady injector response leading to mixing inhomogeneities. Weak secondary waves are pressure wave propagating in a counter-rotating direction compared to one or multiple stronger primary detonation waves in an RDE. These weak waves are also associated with a significantly lower pressure spike. Although not detonation themselves, weak secondary waves interact with the primary detonation waves and with parasitic deflagrations occurring within the combustor. This leads to a precessing pattern of heightened heat release rate regions, which allowed the identification of secondary wave in a number of recent experimental studies [16–19]. The effect of these secondary waves on injector dynamics, mixing, and thermodynamic efficiency however remains an open research question.

The present work focuses on examining injector dynamics in the presence of weak secondary waves. This fundamental issue is investigated by performing a LES of the Air Force Research Laboratory (AFRL) modular RDRE [4, 5, 20–22]. After briefly introducing this configuration (sec. 2) and the numerical setup (sec. 3), we present results of this simulation in sec. 4, and discuss the interaction between primary and secondary waves.

2 The AFRL Rotating Detonation Rocket Engine

The RDRE studied in the present work has been operated for AFRL [5]. We focus on operating conditions corresponding to experiments by Bennowitz et al. [4, 20]: the fuel is gaseous methane, the oxidizer gaseous oxygen, with a total mass-flow rate of $\dot{m}_{tot} = 352 \text{ g s}^{-1}$ and a global equivalence ratio of $\varphi = 1.16$. Simulations of this configuration were reported in previous studies [20–22]. A picture and cross-sectional schematic with key dimensions are shown in Fig. 1. The computational domain used for LES corresponds to that represented in Fig. 1b, and, in addition to the combustion chamber and injection system, includes two upstream annular reactant manifolds and one exhaust plenum.

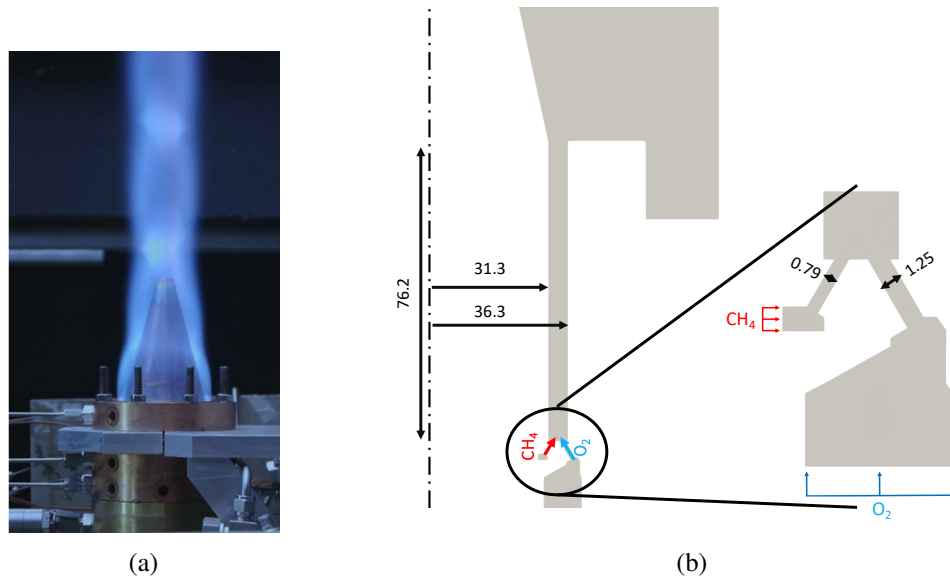


Figure 1: (a) Picture of the RDRE investigated in the present work, reproduced from [4]; (b) Radial cut of the computational domain with key dimensions in mm and zoomed in view of the injection system. The upstream and exhaust plenums have been cut in this representation.

The injectors are cylindrical and angled towards each other by 60° with respect to the injection plane. In this design, the injectors are not choked, but a high velocity is maintained within the reactant streams to avoid backflow [21]. All 72 fuel injectors are connected to a common annular methane manifold. The oxidizer injection system is set-up in a similar manner. The inlet boundary conditions for each manifold are located on their lower wall and the inlet temperature is set to 300 K.

3 Numerical Setup

The numerical setup is similar to that of previous works [23, 24], in which validation and mesh convergence studies were reported. For the reader's convenience, we repeat here the main features of the numerical setup. The computational grid contains a total of 54 million control volumes. Most of the

mesh adopts a block structured topology with hexahedral elements. Tetrahedral elements are used in the fuel and oxidizer manifolds, as well as the upper part of the combustion chamber. Inside the injection system, the typical element size is $50\ \mu\text{m}$. In the lower part of the combustion chamber, where the detonations occur, elements range in size from $50\ \mu\text{m}$ to $80\ \mu\text{m}$. The fully compressible finite-volume solver described in [25] is used, with a 4th-order accurate special discretization scheme for the mass, momentum, and energy conservation equation. A simple-balancing splitting scheme for the advection-diffusion-reaction equations is used to increase the convective timestep to a typical value of 5 ns [26]. The stiff reaction time-stepping is treated with a fourth-order semi-implicit Rosenbrock-Krylov scheme while the non-stiff advection/diffusion operators are solved using a third-order strong stability preserving Runge-Kutta scheme. A 1st order scheme is used in the regions surrounding shock waves and detonation, using two shock sensors: one based on pressure and density gradients to avoid numerical instabilities; and one based on species mass fraction and temperature to avoid overshoot/undershoot. Chemistry is modeled using a multi-species finite-rate chemistry approach with the 12 species, 38 reactions FFCMy-12 mechanism specifically designed for high pressure oxy-methane rocket engine combustion [27]. All walls in the domain are treated as no-slip and adiabatic. The inlet and outlet boundary conditions use the Navier-Stokes Characteristic Boundary Conditions method [28] with values for the relaxation coefficients that ensure a non-reflective acoustic behavior. Turbulent subgrid stresses (SGS) are represented using the Vreman model.

4 Results and discussion

We first compare global quantities of interest (QoI) from our simulation to measurements obtained during experiments conducted by Bennowitz et al. [4, 20]. Results are summarized in Table 1. In both experiment and simulation, all detonation waves are co-rotating. However, one less wave is found in the LES. This discrepancy in number of waves explains the lower detonation velocity observed in the LES. Other metrics of interest, namely the thrust, specific impulse (ISP), and mean static pressure at the outer wall (measured at axial positions $y = 8.9\ \text{mm}$, CTAP1, and $y = 28.6\ \text{mm}$, CTAP2, using capillary tube attenuated pressure sensors) are in good agreement between the LES and experiment.

Table 1: Comparison of quantities of interest to experimental data.

QoI	Experiment	LES	Difference
# waves	3	2	-33.3%
U_{det} [m/s]	1668	1264	-24%
CTAP1 [MPa]	0.50	0.52	4.0%
CTAP2 [MPa]	0.43	0.42	-2.3%
Thrust [lbf]	132	136	-3.2%
ISP [s]	164	175	-6.7%

Space-time ($\theta - t$) diagrams are a powerful and well-established tool to study wave and combustion dynamics within rotating detonation systems [29]. These diagrams are obtained by volume-averaging quantities of interests over wedges, with a 1° extent in azimuthal direction, and $0 \leq y \leq 20\ \text{mm}$ extent in the axial direction. Wedges extend over the entire width of the annular combustor. Capitalized notations \bar{P} and \bar{Q} are utilized to denote this wedge-averaging process.

Figure 2 shows these $\theta - t$ diagrams for pressure \bar{P} and heat release rate \bar{Q} . Two primary waves, co-rotating in the clockwise direction and separated by approximately 160° are clearly distinguishable.

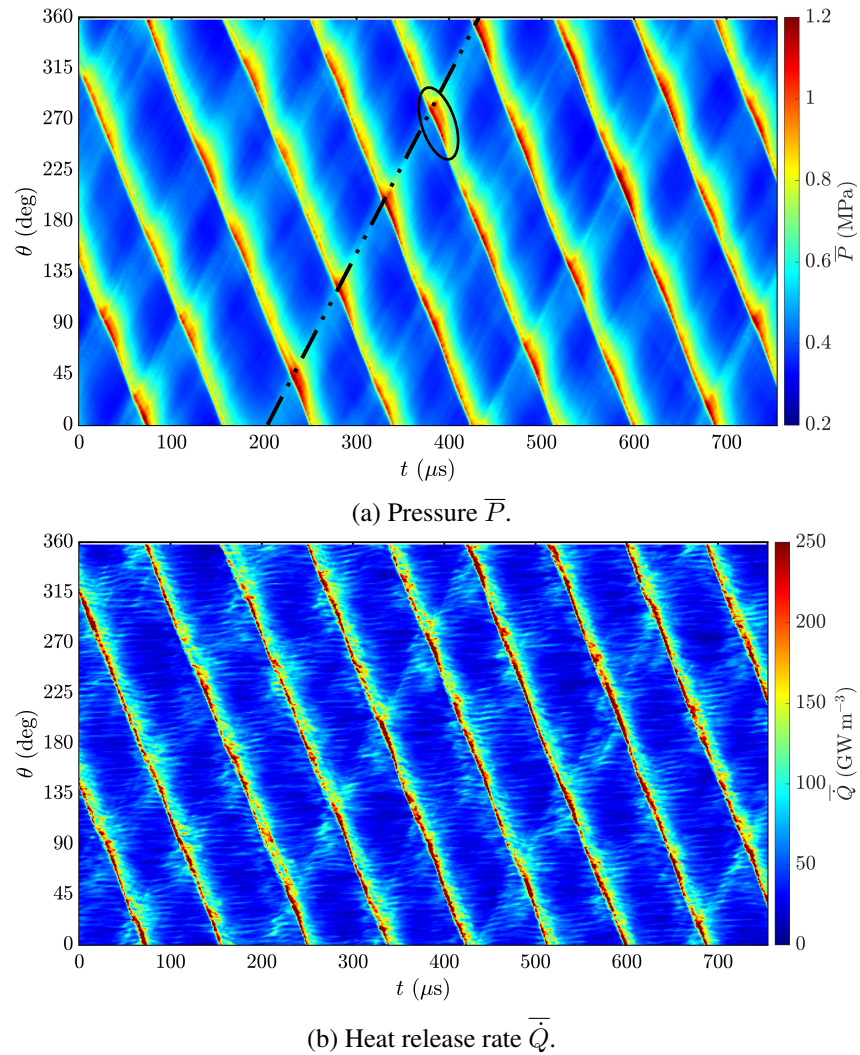
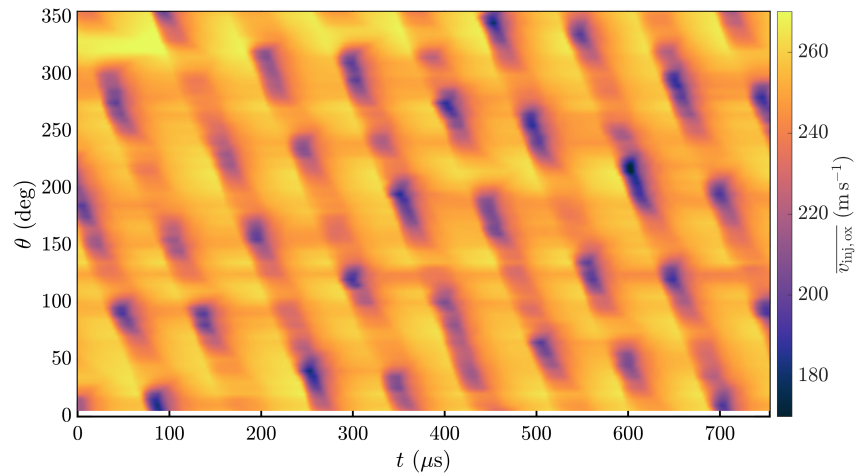
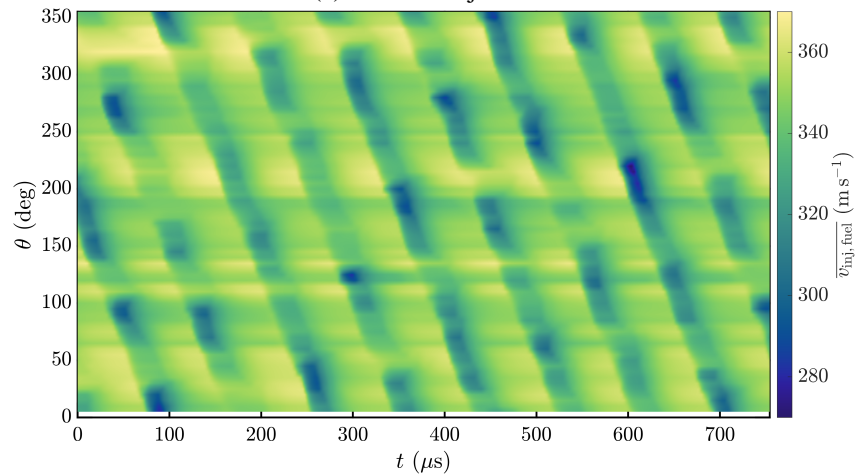


Figure 2: Space-time diagram ($\theta - t$) showing the wave dynamics. Pressure and heat release rate are averaged over radial, axial ($0 < z < 20$ mm) and azimuthal (1° increments) directions. The two main detonation waves are visible as clockwise rotating (downward slanted) patterns, the two secondary counter-clockwise rotating waves are visible as weaker, upward slanted patterns. A black dashed line is used in (a) to illustrate such a secondary wave. A region of interaction between a main wave and a secondary wave, characterized by a localized increase in pressure rise, is illustrated in (a) by a black ellipse.



(a) Oxidizer injectors.



(b) Fuel injectors.

Figure 3: Space-time diagram ($t - \theta$) of the sectional-averaged injector velocity in the (a) oxidizer and (b) fuel injector port. Patches corresponding to a higher blockage and a higher velocity deficit match well with the pattern visible in the pressure diagram, Fig. 2a, illustrating the significant impact of secondary waves on injector dynamics.

High heat release rate, in the order of 300 GW m^{-3} , is found immediately downstream of these primary wave, indicating the pressure gain combustion nature of these waves. In addition to these two primary waves, one can distinguish two counter-rotating secondary weak waves. One of these is highlighted with a black dotted line in Fig. 2a. The pressure peak and heat release rate associated with these secondary waves are significantly weaker, except in regions where primary and secondary waves interact. In these localized regions, peaks in pressure rise are significant: on the order of 1.2 MPa, and these are accompanied by high heat release rates. These regions form a somewhat regular pattern, with a marked precession of approximately 55° per full rotation of the detonations. This behavior was also reported in [15, 17].

Fig. 3 focuses on the injector dynamics arising from this complex, multi-wave behavior, using $\theta - t$ diagrams. In Fig. 3, the azimuthal coordinate θ indexes the position of injectors within the system, and the diagrams report the cross-sectional averaged velocity within the oxidizer (Fig. 3a) and fuel injectors (Fig. 3b). Following the passage of primary waves, the increase in chamber pressure causes a decrease in injector velocity, by an average of 11% in oxidizer injectors and 8% in fuel injectors. In both streams, the injector recovery time is $54 \mu\text{s}$. These behaviors are well-known and characterized in previous studies [3, 15, 21]. In Fig. 3, a more unusual pattern is however clearly visible: localized regions of higher injector velocity deficit are present in regions where primary and secondary waves interact, with up to 27% (resp. 21%) velocity deficit in the oxidizer (resp. fuel) injector during primary-secondary wave interaction. Moderately higher chamber pressures during these interactions, and the non-linear response of the injection system leads to this significantly higher injector blockage. This will in turn affect reactant filling, mixing, and combustion within a few sectors of the RDRE.

5 Conclusions

A large eddy simulation of the modular rotating detonation rocket engine of the Air Force Research Laboratory is conducted using a multi-species finite rate chemistry approach to model methane-oxygen combustion. At the operating condition under investigation, two strong co-rotating primary waves and two weak contra-rotating secondary waves are found within the combustor. We find that when strong and weak waves interact, higher chamber pressure are achieved, leading to a locally higher heat release rate and a significant (2.5 times) reduction in velocity within the injection ports compared to the typical injector blockage for this configuration. The strong effects of primary-secondary wave interaction on chamber pressure, injection dynamics, and combustion could lead to a significantly different behavior for a few sectors within an RDRE, leading to potentially detrimental imbalances within the engine, which will be examined in future work.

Acknowledgements

This work was supported by the Air Force Office of Scientific Research (AFOSR) under award number FA9550-21-1-0077 with Chiping Li as program manager. This research used resources of the National Energy Research Scientific Computing Center, a U.S. Department of Energy Office of Science User Facility operated under Contract No. DE-AC02-05CH11231.

References

- [1] F. K. Lu, E. M. Braun, and J. Powers, "Rotating detonation wave propulsion: Experimental challenges, modeling, and engine concepts," *Journal of Propulsion and Power*, vol. 30, no. 5, pp. 1125–1142, 2014.

- [2] P. Wolański, “Detonative propulsion,” *Proceedings of the Combustion Institute*, vol. 34, no. 1, pp. 125–158, 2013.
- [3] B. A. Rankin, M. L. Fotia, A. G. Naples, C. A. Stevens, J. L. Hoke, T. A. Kaemming, S. W. Theuerkauf, and F. R. Schauer, “Overview of performance, application, and analysis of rotating detonation engine technologies,” *Journal of Propulsion and Power*, vol. 33, no. 1, pp. 131–143, 2017.
- [4] J. W. Bennewitz, B. R. Bigler, W. A. Hargus, S. A. Danczyk, and R. D. Smith, “Characterization of detonation wave propagation in a rotating detonation rocket engine using direct high-speed imaging,” in *Proceedings of the AIAA Joint Propulsion Conference*, ser. AIAA paper 2018-4688, 2018.
- [5] R. D. Smith and S. B. Stanley, “Experimental investigation of rotating detonation rocket engines for space propulsion,” *Journal of Propulsion and Power*, vol. 37, no. 3, pp. 463–473, 2021.
- [6] K. Goto, Y. Kato, K. Ishihara, K. Matsuoka, J. Kasahara, A. Matsuo, I. Funaki, D. Nakata, K. Higashino, and N. Tanatsugu, “Thrust validation of rotating detonation engine system by moving rocket sled test,” *Journal of Propulsion and Power*, vol. 37, no. 3, pp. 419–425, 2021.
- [7] J. Kindracki, P. Wolański, and Z. Gut, “Experimental research on the rotating detonation in gaseous fuels-oxygen mixtures,” *Shock Waves*, vol. 21, no. 2, pp. 75–84, 2011.
- [8] K. Goto, R. Yokoo, A. Kawasaki, K. Matsuoka, J. Kasahara, A. Matsuo, I. Funaki, and H. Kawashima, “Investigation into the effective injector area of a rotating detonation engine with impact of backflow,” *Shock Waves*, vol. 31, no. 7, pp. 753–762, 2021.
- [9] K. Goto, K. Matsuoka, K. Matsuyama, A. Kawasaki, H. Watanabe, N. Itouyama, K. Ishihara, V. Buyakofu *et al.*, “Flight Demonstration of Detonation Engine System Using Sounding Rocket S-520-31: Performance of Rotating Detonation Engine,” in *Proceedings of the AIAA SciTech Forum*, ser. AIAA paper 2022-0232, 2022.
- [10] R. Yokoo, K. Goto, J. Kim, A. Kawasaki, K. Matsuoka, J. Kasahara, A. Matsuo, and I. Funaki, “Propulsion performance of cylindrical rotating detonation engine,” *AIAA Journal*, vol. 58, no. 12, pp. 5107–5116, 2020.
- [11] S. J. Liu, Z. Y. Lin, W. D. Liu, W. Lin, and F. C. Zhuang, “Experimental realization of H₂/Air continuous rotating detonation in a cylindrical combustor,” *Combustion Science and Technology*, vol. 184, no. 9, pp. 1302–1317, 2012.
- [12] J. E. Shepherd and J. Kasahara, “Analytical Models for the Thrust of a Rotating Detonation Engine. California Institute of Technology, GALCIT report FM2017.001,” 2017. [Online]. Available: https://authors.library.caltech.edu/81786/1/rde_model_report.pdf
- [13] J. Sousa, G. Paniagua, and E. Collado Morata, “Thermodynamic analysis of a gas turbine engine with a rotating detonation combustor,” *Applied Energy*, vol. 195, pp. 247–256, 2017. [Online]. Available: <http://dx.doi.org/10.1016/j.apenergy.2017.03.045>
- [14] T. Kaemming, M. L. Fotia, J. Hoke, and F. Schauer, “Thermodynamic modeling of a rotating detonation engine through a reduced-order approach,” *Journal of Propulsion and Power*, vol. 33, no. 5, pp. 1170–1178, 2017.
- [15] V. Raman, S. Prakash, and M. Gamba, “Non idealities in rotating detonation engines,” *Annual Review of Fluid Mechanics*, vol. 55, pp. 639–674, 2023.
- [16] F. Chacon, A. D. Feleo, and M. Gamba, “Secondary waves dynamics and their impact on detonation structure in rotating detonation combustors,” *Shock Waves*, vol. 31, no. 7, pp. 675–702, Oct. 2021. [Online]. Available: <https://doi.org/10.1007/s00193-021-01034-6>

- [17] M. D. Bohon, A. Orchini, R. Bluemner, C. O. Paschereit, and E. J. Gutmark, "Dynamic mode decomposition analysis of rotating detonation waves," *Shock Waves*, vol. 31, no. 7, pp. 637–649, 2021.
- [18] X. Huang, C. J. Teo, and B. C. Khoo, "Experimental investigation on coexisting wave components in an optically accessible rotating detonation combustor," *Aerospace Science and Technology*, vol. 111, p. 106538, 2021.
- [19] C. L. Journell, R. M. Gejji, I. V. Walters, A. I. Lemcherfi, C. D. Slabaugh, and J. B. Stout, "High-speed diagnostics in a natural gas–air rotating detonation engine," *Journal of Propulsion and Power*, vol. 36, no. 4, pp. 498–507, 2020.
- [20] C. F. Lietz, Y. Desai, o. Hargus, and V. Sankaran, "Parametric investigation of rotating detonation rocket engines using large eddy simulations," in *Proceedings of the AIAA Propulsion and Energy Forum*, ser. AIAA paper 2019-4129, 2019.
- [21] S. Prakash, V. Raman, C. F. Lietz, W. A. Hargus, and S. A. Schumaker, "Numerical simulation of a methane-oxygen rotating detonation rocket engine," *Proceedings of the Combustion Institute*, vol. 38, no. 3, pp. 3777–3786, 2021.
- [22] A. Batista, M. C. Ross, C. Lietz, and W. A. Hargus, "Descending modal transition dynamics in a large eddy simulation of a rotating detonation rocket engine," *Energies*, vol. 14, no. 12, pp. 1–22, 2021.
- [23] D. Brouzet, G. Vignat, and M. Ihme, "Dynamics and structure of detonations in stratified product-gas diluted mixtures," *Proceedings of the Combustion Institute*, 2023.
- [24] G. Vignat, D. Brouzet, and M. Ihme, "Effect of preburn inhomogeneities on the detonation velocity in a rotating detonation rocket engine," in *Proceedings of the 28th International Conference on Detonations, Explosions, and Reactive Systems*, 2022.
- [25] P. C. Ma, Y. Lv, and M. Ihme, "An entropy-stable hybrid scheme for simulations of transcritical real-fluid flows," *Journal of Computational Physics*, vol. 340, pp. 330–357, 2017.
- [26] H. Wu, P. C. Ma, and M. Ihme, "Efficient time-stepping techniques for simulating turbulent reactive flows with stiff chemistry," *Computer Physics Communications*, vol. 243, pp. 81–96, 2019.
- [27] R. Xu, K. Wang, S. Banerjee, J. Shao, T. Parise, Y. Zhu, S. Wang, A. Movaghar *et al.*, "A physics-based approach to modeling real-fuel combustion chemistry – II. Reaction kinetic models of jet and rocket fuels," *Combustion and Flame*, vol. 193, pp. 520–537, 2018.
- [28] T. Poinso and S. K. Lele, "Boundary conditions for direct simulations of compressible viscous flows," *Journal of Computational Physics*, vol. 101, pp. 104–129, 1992.
- [29] J. W. Bennewitz, B. R. Bigler, S. A. Schumaker, and W. A. Hargus, "Automated image processing method to quantify rotating detonation wave behavior," *Review of Scientific Instruments*, vol. 90, no. 6, 2019.